Journal of
MATERIALS RESEARCH

Optical properties of MS_2 (M = Mo, W) inorganic fullerene-like and nanotube material optical absorption and resonance Raman measurements

G. L. Frey and R. Tenne
Department of Materials and Interfaces, Weizmann Institute, Rehovot 76100, Israel

M. J. Matthews, M. S. Dresselhaus, and G. Dresselhaus
Department of Physics, Massachusetts Institute of Technology, Cambridge, Massachusetts 02139

(Received 6 February 1998; accepted 7 May 1998)

The optical properties of inorganic fullerene-like and nanotube MS_2 (M = Mo, W) material are studied through absorption and resonance Raman, and compared to those of the corresponding bulk material. The absorption measurements show that the semiconductivity is preserved. Nevertheless, the positions of the excitons are altered in comparison to the bulk. The Raman spectra of the nanoparticles show a close correspondence to that of the bulk. However, the first-order peaks are broadened and, under resonance conditions, new peaks are observed. The new peaks are assigned to disorder-induced zone edge phonons.

I. INTRODUCTION

Carbon fullerenes and nanotubes have been investigated intensively in the last few years. The driving force for their formation is the instability of nanoscopic planar graphene sheets. In analogy to that, it was suggested that nanoscopic planar sheets of layered dichalcogenides and other layer compounds are unstable and would transform, under appropriate conditions, into caged structures.[1] This concept extends the scope of fullerene-like materials into inorganic solid state compounds. Consequently, an abundance of other fullerene-like or nanotube materials have been produced and studied in recent years. The first inorganic compounds to exhibit fullerene-like structures were the layered metal dichalcogenides MX_2 (M = Mo, W; X = S, Se), generically called *inorganic fullerene-like material-IF*[1,2] (see Fig. 1). Subsequently, the large-scale synthesis of IF-MS_2 (M = Mo, W) powder has been reported.[3–5] Furthermore, these IF metal dichalcogenides exhibit a variety of sizes and shapes and have been investigated by x-ray powder diffraction (XRD),[3] scanning tunneling microscopy (STM),[6] high resolution transmission electron microscopy (TEM),[3–5] optical absorption spectroscopy,[7] and Raman scattering.[8] The XRD analysis revealed that the bulk 2H structure of the unit cell is locally preserved within an IF particle. Nonetheless, a shift of the XRD (0002) peak of the IF phase indicates a lattice expansion of ca. 2% between two adjacent MS_2 slabs along the *c*-axis compared to the bulk 2H polytype.[4] This expansion is attributed to the strain in the bent layers and to discommensuration between layers of different radii, i.e., different number of atoms.

In this paper we present a comprehensive study of the optical absorption and resonance Raman (RR) spectra of the MS_2 fullerene-like and nanotube materials, and compare them to those of the analogous 2H bulk. Although the optical properties of the caged structures resemble those of their respective single crystals, the present study is nevertheless important for understanding the structure-property relationships in more detail.

II. EXPERIMENTAL

The synthesis of IF-MS_2 and MS_2-nanotubes has been previously reported.[3–5] Briefly, a starting precursor of MO_3 powder is heated to temperatures above 800 °C and is reduced to MO_{3-x} in a reducing atmosphere (typically 5% H_2/95% N_2; 100 ml/min). The suboxide reacts with H_2S gas (4 ml/min) which converts the suboxide particle into the respective IF-MS_2 nanoparticle. The reaction product is collected in powder form on a quartz substrate. The diameter of the IF-MS_2 quasispherical (polyhedral) particles, as characterized by TEM analysis, ranged from 200 to 2000 Å. The length of the MS_2 nanotubes ranged from 1500 to 3000 Å, and the diameter

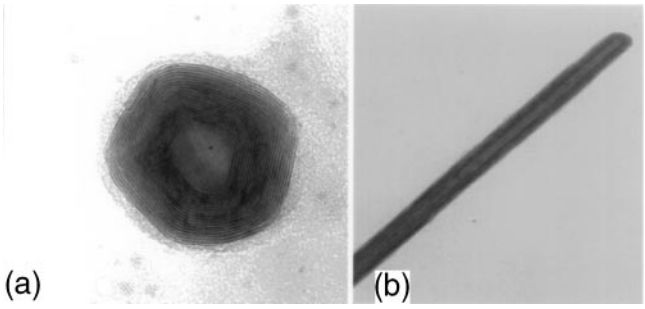

FIG. 1. TEM micrographs of (a) typical IF-MoS_2 particle and (b) typical WS_2 nanotube. The distance between two fringes (MS_2 layer) is 6.2 Å.

of their cross section was 150–200 Å. The synthesis procedure does not provide full control of the size and shape of the particles, and hence a 10% size distribution is obtained in each sample. Selected area (<50 Å) energy dispersive x-ray analysis of single nanoparticles gave a stoichiometric ratio of 1 : 2 for Mo : S.

Optical absorption spectral measurements over the range of 400–800 nm (1.6–3 eV) were carried out on films containing over 80% IF with a 10% size distribution. A standard setup was used, equipped with a tungsten lamp, double grating monochromator (Jobin-Yvon HRD), liquid helium cryostat (TBT), and cooled photomultiplier (Hammamatsu RG942). The temperature was varied between 4.2 and 300 K. Careful background subtraction was performed. The accurate positions of the A and B excitons were deduced from the spectra by a Gaussian fitting procedure.

For the resonance Raman (RR) spectra, the 6328 Å (1.96 eV) line of a He/Ne laser was used, capable of supplying 1 mW of power. Several locations on each sample surface were probed to ensure reproducibility of the data. The RR experiments were done on a Dual Renishaw micro-Raman system 1000 instrument.

III. RESULTS AND DISCUSSION

A. Optical absorption

After annealing the molybdenum oxide film for 3 min, the particles formed are 350 ± 50 Å in diameter, and consist of an oxide core and a few closed sulfide layers (<10), as shown in Fig. 2(a). Subsequent annealing for 90 min at the same temperature leads to a complete conversion of the oxide into an IF-MoS_2 with many layers (>10), as shown in Fig. 2(b). The absorption spectra of the same IF-MoS_2 sample, after 3 and 90 min annealing (sulfidization), are shown in curves 1 and 2 of Fig. 2(c), respectively. They are compared to the spectrum of 2H-MoS_2 bulk at the same temperature (25 K) [curve 3 of Fig. 2(c)].

2H bulk MoS_2 and WS_2 are indirect gap semiconductors with two series of exciton absorption bands, A and B, at the absorption edge.[9,10] The optical transitions in 2H-MoS_2 and 2H-WS_2 are summarized in Table I. Quantum confinement of carriers was also studied in transition metal dichalcogenides. Their characteristic layered structure leads to a quantization effect along the *c*-axis (perpendicular to the layers) in ultrathin films[14–16] and to a quantum size effect in nanoparticles <45 Å.[17,18]

Figure 2 reveals that the semiconductivity of the layered material is preserved in the IF structures. Nevertheless, after annealing for 3 min, the energies of the A and B excitons are lowered by 25 and 80 meV, respectively, compared to the 2H-MoS_2 bulk material. Additional annealing (90 min) did not influence the average size of the IF, but added more sulfide layers at the expense of the oxide core. However, the additional annealing leads to a further decrease of the exciton energy: 40 and 100 meV for the A and B excitons, respectively, compared to the bulk 2H material. A similar

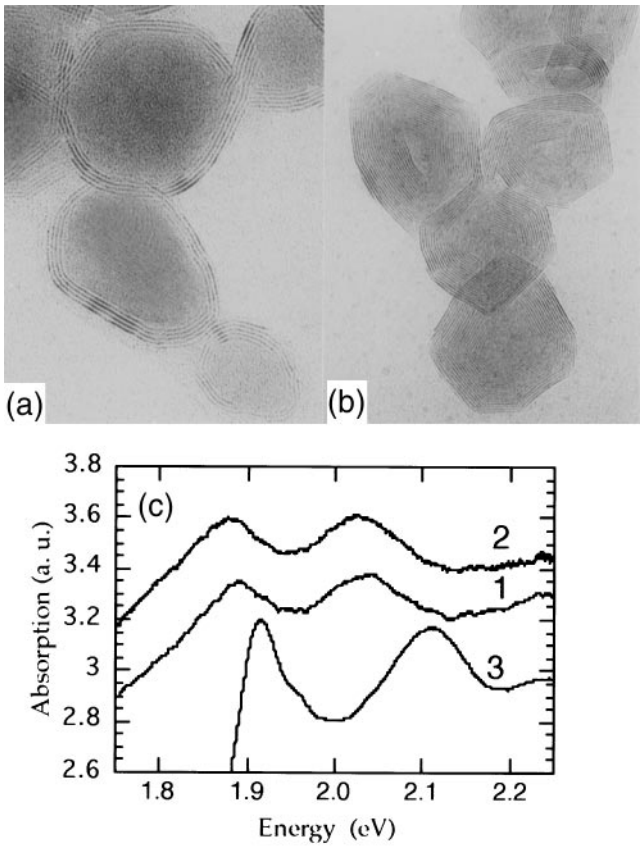

FIG. 2. (a) TEM micrograph of an IF-MoS_2 sample after 3 min annealing. The nanoparticles consist of an oxide core and a few IF layers ($n < 10$) are seen. (b) TEM micrograph of the same sample as in (a) after 90 min of annealing. The oxide is fully converted into IF-MoS_2 with many layers ($n > 10$). The distance between two fringes (MoS_2 layer) is 6.2 Å. (c) The optical absorption spectra at 25 K of the above MoS_2 samples, curves (1) and (2), are of the samples shown in (a) and (b), respectively. Curve (3) is the absorption spectrum of bulk 2H-MoS_2.

TABLE I. Optical transitions in 2H-MoS_2 and 2H-WS_2 at various temperatures. The room temperature values correspond to those found in (a) Ref. 10, (b) Ref. 11, (c) Ref. 12, and (d) Ref. 13.

Material	Temp. (K)	Indirect band gap (eV)	Direct band gap (eV)	A exciton position (eV)	B exciton position (eV)
2H-MoS_2	300	1.2[a]	1.95[c]	1.88[d]	2.06[d]
	150			1.90	2.10
	75			1.91	2.11
	25			1.91	2.11
2H-WS_2	300	1.3[b]	2.05[b]	1.95[b]	2.36[b]
	150			2.10	2.40
	75			2.05	2.45
	25			2.05	2.45

red shift of the A and B exciton energies of IF-MoS_2 has been observed at all studied temperatures (4–300 K). The same trend was observed in the absorption spectra of an IF-WS_2 > 1000 Å sample. After 6 min annealing, the IF-WS_2 are introduced into ethanol to form an alcoholic suspension. At room temperature, the spectra of the suspension shows that the A and B excitons are, respectively, 10 and 30 meV red shifted compared to the 2H bulk spectra and are at 1.94 and 2.33 eV, respectively. Further red shifts of 30 and 80 meV for the A and B excitons, respectively, are observed upon further annealing for 120 min (the A and B exciton positions are now at 1.91 and 2.25 eV, respectively). Similar red shifts of the A and B excitons were observed for all IF-MS_2 samples with more than 6–7 layers at all detected temperatures. This decrease is consistent with the smaller indirect gap measured for a single IF-MoS_2 nanoparticle using STM.[6]

In addition to the red shift of the excitons, a broadening of the peaks and a tailing of the absorption edge to lower energies is observed. These effects may be attributed, at least partially, to the fairly large size and shape distribution of the particles. Whether these effects are intrinsic to the IF particles could be determined when the synthesis of the particles is better controlled and more uniform samples are available. Nevertheless, the red shift observed seems to be inherent to the topology of the IF structure with many shells.[7]

To study quantum effects in the direction perpendicular to the S–M–S layers, Consadori and Frindt[15] followed the behavior of the A exciton ground state energy (exciton binding energy ≈ 50 meV), in ultrathin films of 2H-WSe_2 of thickness 13 Å < L_z < 500 Å, where L_z is the film thickness. For film thicknesses in the range of 80–500 Å ($12 < n < 90$), where n is the number of atomic layers, the exciton energy was independent of the film thickness. For film thicknesses in the range of 40–70 Å ($6 < n < 11$), a linear dependence of the exciton energy on $1/L_z^2$ was found, and assigned to a quantization effect in the z direction:

$$\Delta E_g \approx \frac{\pi^2 \hbar^2}{\mu_{\parallel} L_z^2}, \qquad (1)$$

where E_g is the bandgap and $\mu_{\parallel}$ is the exciton effective mass in the direction parallel to the c-axis. For platelets less than 40 Å thick, the dependence of the A exciton peak on thickness is much weaker and cannot be accounted for by Eq. (1). Accordingly, in Fig. 3, the A and B exciton energies of IF-MoS_2 and IF-WS_2 are plotted versus $1/L_z^2$ ($L_z = n_* 6.3$ Å) at 25 K. In sharp contrast to the 2H-WSe_2 thin films studied by Consadori and Frindt,[15] here thick films (500–1500 Å) consisting of nanoparticles <1500 Å (IF), but with various MS_2 "shell" thicknesses, are measured. Figure 3

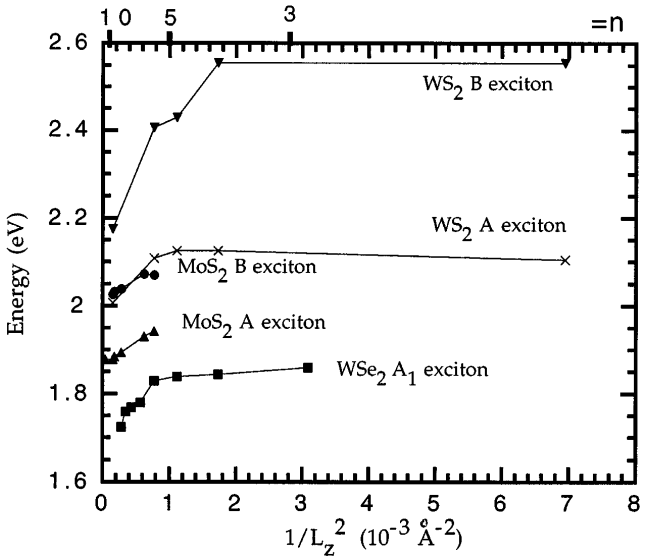

FIG. 3. Plot of the A and B exciton energies of IF-MoS_2 and IF-WS_2 vs $1/L_z^2$. (▲) and (●) represent the data for the A and B excitons of IF-MoS_2, respectively; (×) and (▼) show the data for the A and B excitons of IF-WS_2. (■) represents the A exciton of 2H-WSe_2 at 77 K.[15]

reveals two important results: (i) a linear dependence of the excitons' energies on $1/L_z^2$ was found also for IF material in the (shell) thickness range 35–80 Å ($6 < n < 12$, $0.15 < 1000/L_z^2 < 0.75$) similar to that found in thin films. (ii) For IF with $L_z > 80$ Å ($n > 10$), the excitons' energies are thickness independent and saturate at a constant value,[7] which is smaller than the exciton energies obtained for the corresponding single crystals (as mentioned earlier). For IF-MoS_2 (value for 2H bulk samples are in parentheses) at room temperature, the A exciton value is at 1.82 (1.88) eV and the B exciton value is at 1.95 (2.06) eV. For IF-WS_2 at room temperature, the A exciton position is 1.91 (1.95) and the B exciton is down shifted to 2.26 (2.36) eV. For both IF-MoS_2 and IF-WS_2, the red shift of the A exciton energy compared to that of the 2H polytype is smaller than that obtained for the B exciton.

Ideally, a lattice expansion of the bulk 2H-MS_2 crystal between two adjacent MS_2 slabs along the c-axis leads effectively to a 2D MS_2 single layer, with a trigonal prism coordination of the Mo atoms. Unfortunately, this single-layer structure is unstable. Band structure calculations for such a single S–Mo–S sandwich were performed by Kobayashi *et al.*,[19] using the linear combination of atomic orbitals (LCAO) method. The influence of the lattice expansion is seen in some of the band dispersion curves, but attention is here focused on the smallest direct gap at the K point, especially the K_1 and K_4 exciton initial states. For a MoS_2 single-layer nanofilm, the splitting of the A and B exciton initial states no longer exists, and the two states are degenerate. The convergence of K_1 and K_4 into one band occurs by

lowering the energy of the K_4 band (the A exciton initial state), and increasing the energy of the K_1 band (the B exciton initial state).[7] Therefore, for an intermediate state, where the *c*-axis expands but the 2D system is not yet reached, this process should come into view as a blue shift of the A exciton and a red shift of the B exciton in the absorption spectra, until, for a single layer, the two peaks merge into a single peak. Nanotubes, with few atomic layers and a lattice expansion between two adjacent MS_2 slabs along the *c*-axis compared to the 2H bulk, are a system with close correspondence to the unstable single-layer structure. Indeed, in the optical absorption spectrum of WS_2 nanotubes with 1 or 2 layers and 4% expansion along the *c*-axis,[5] an increase of 20 meV in the A exciton energy, and a decrease of 130 meV in the B exciton energy, are observed as shown in Fig. 4.

TABLE II. Raman peaks observed in 2H-MoS_2 bulk and IF-MoS_2. The spectra are excited at 6328 Å, and the corresponding symmetry assignments are listed. All peak positions are in cm^{-1}.

Bulk MoS_2	IF-MoS_2 (800 Å)	IF-MoS_2 (200 Å)	Symmetry assignment
177	182	182	$A_{1g}(M) - LA(M)$
	228	228	$LA(M)$
	250	250	edge phonon
287		286	$E_{1g}(\Gamma)$
383	383	381	$E^1_{2g}(\Gamma)$
409	409	409	$A_{1g}(\Gamma)$
421[10]	weak	weak	
466	455	455	$2 \times LA(M)$
	498	498	edge phonon
529	weak		$E_{1g}(M) + LA(M)$
572	567	567	$2 \times E_{1g}(\Gamma)$
607	593	593	$E^1_{2g}(M) + LA(M)$
643	636	636	$A_{1g}(M) + LA(M)$

B. Resonance Raman spectroscopy

The Raman spectra of 2H-MoS_2 and 2H-WS_2 bulk crystals have been studied extensively.[20–22] A group-theoretical analysis of the lattice vibrations at the Γ point in the hexagonal Brillouin zone (BZ) has been previously published.[23] There are four Raman-active modes corresponding to the following symmetries: E^2_{2g}, E_{1g}, E^1_{2g}, and A_{1g} (for the mode frequencies of MoS_2 and WS_2 see Tables II and III, respectively). The E^2_{2g} phonon is associated with the vibration of one MS_2 layer against its neighboring layers and is called the rigid-layer mode. In backscattering experiments on a surface perpendicular to the *c*-axis, the E_{1g} mode is forbidden. The RR spectra of bulk 2H-MoS_2 and 2H-WS_2 have been reported using laser energies near the absorption edge.[22,24,25] The RR scattering of the bulk 2H material was analyzed in terms of second-order-Raman (SOR) scattering due to the coupling of the phonon modes to electronic transitions associated with either the band gap or the excitonic states.

Using the 4880 and 5145 Å laser line excitations, the Raman spectra of MoS_2 nanoparticles, in the form of inorganic fullerene-like (IF) and platelet (PL) samples, showed that by decreasing the crystallite dimensions, the linewidths of the first-order Raman modes are broadened.[8] The broadening effect was explained in terms of modifications to the space correlation function brought about by the finite crystallite size.

TABLE III. Raman peaks observed in 2H-WS_2 bulk, IF-WS_2, and nanotubes. The spectra are excited at 6328 Å, and the corresponding symmetry assignments are listed. All peak positions are in cm^{-1}.

Bulk WS_2[25]	IF-WS_2 1200–1500 Å	WS_2 nanotubes 200 × 2000 Å	Symmetry assignment
	152	153	
172	172	172	$E^1_{2g}(M) - LA(M)$; $LA(M)$
193	192	192	
212	210	210	
229	229	230	$A_{1g}(M) - LA(M)$
week	263	262	$2LA(M) - 3E^2_{2g}(M)$
294	294	294	$2LA(M) - 2E^2_{2g}(M)$
348	350	350	$2 \times LA(M)$; $E^1_{2g}(\Gamma)$
381	381	381	$2LA(M) + 2E^2_{2g}(M)$
418	417	416	$A_{1g}(\Gamma)$
444 (shoulder)	438 (shoulder)	438 (shoulder)	
476	475	475	$E_{1g}(M) + LA(M)$
521	521	521	$E^1_{2g}(M) + LA(M)$
544	547	548	
580	580	581	$A_{1g}(M) + LA(M)$
695	695	695	$4xLA(M)$
766	764	767	$A_{1g}(\Gamma) + E^1_{2g}(\Gamma)$
827	829	829	$2xA_{1g}(\Gamma)$

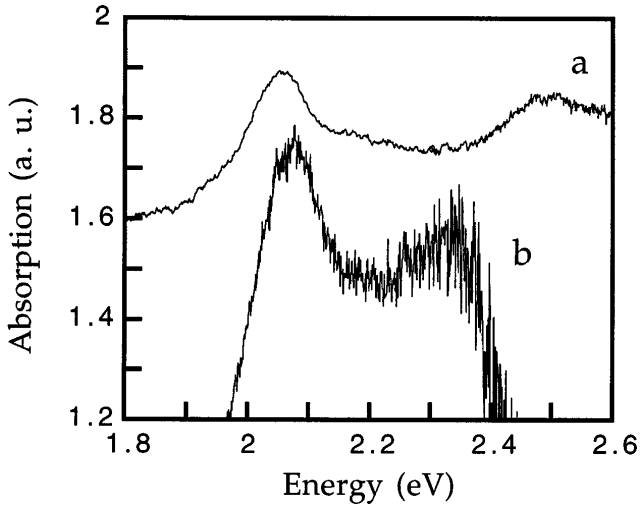

FIG. 4. Absorption spectra at 25 K of (a) 2H-WS_2 bulk and (b) WS_2 nanotubes 150–200 Å in diameter and 1500–3000 Å in length, with 1–2 layers.

Figures 5 and 6 show the RR spectra of MoS_2 and WS_2 nanoparticles, respectively, at a laser excitation wavelength of 6328 Å (1.96 eV). Along with the E^1_{2g} and A_{1g} peaks, many other peaks are observed as a result of the resonance with the allowed electronic transitions. The resulting phonon peak frequencies are tabulated in Table II for MoS_2 and in Table III for WS_2. From the comparison to the corresponding spectra of the 2H bulk samples, it is evident that, in addition to the broadening of the peaks, new Raman peaks are observed at 228, 250, 498 cm^{-1} for IF-MoS_2 and at 152 cm^{-1} for IF and nanotubes of WS_2.

Previous RR[23,24] and inelastic neutron scattering (INS)[26] studies have revealed that second-order processes involving the $LA(M)$ phonon could be used to explain the intense ~460 cm^{-1} peak and other weaker peaks observed in the second-order Raman (SOR) spectra of MoS_2 bulk crystals. Both RR and INS studies found the frequency of the $LA(M)$ phonon in question to be ~230 cm^{-1}. Stacy *et al.* were also able from SOR spectra to estimate the frequency of the M-point optical mode (corresponding to the same branch as the zone center A_{1g} mode) to be 410 cm^{-1}, close to the INS result of 397 cm^{-1}. Using similar arguments (and adapting the notation used in Ref. 24), we can also deduce the frequencies of various BZ edge phonons. Thus, by considering several multiphonon peaks, we find that the frequency of the $LA(M)$ phonon in the nanoparticle samples is about 228 cm^{-1}, which is slightly lower than the previously reported result.[24] Thus, we believe that the peak observed at 228 cm^{-1} is a disorder-induced peak arising from $LA(M)$ phonons.

For WS_2, the RR and inelastic neutron scattering (INS)[25] studies position the non-zone-center LA mode at 352 cm^{-1}. Similar to the analysis done for the RR

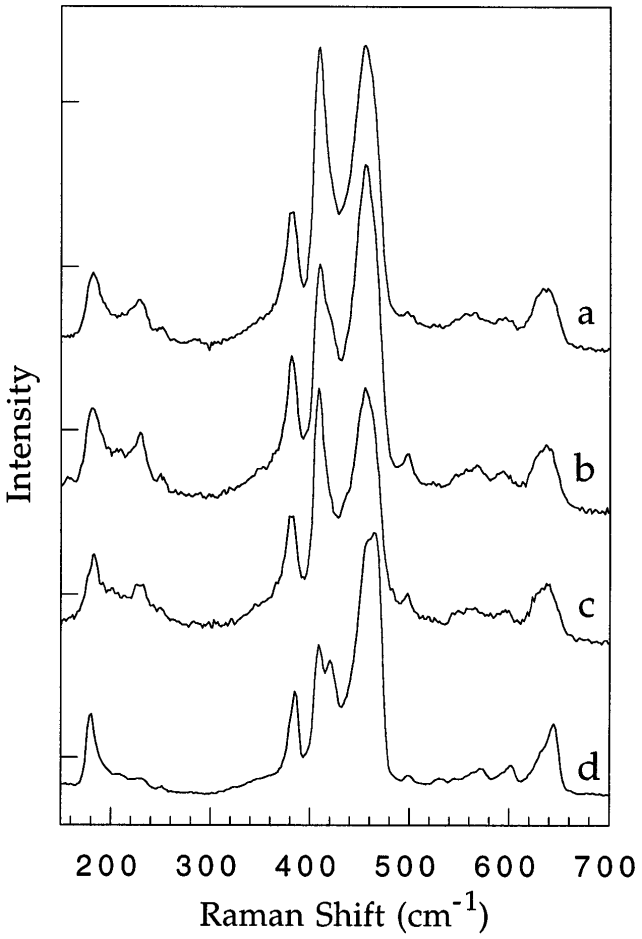

FIG. 5. Resonance Raman (RR) spectra excited by the 6328 Å (1.96 eV) laser line showing SOR bands of several MoS_2 nanoparticle samples: IF-MoS_2 200 Å (a); IF-MoS_2 800 Å (b); PL-MoS_2 50 × 300 $Å^2$ (c); PL-MoS_2 5000 Å (d).

scattering of MoS_2 nanoparticles, the assignments of all multiphonon scattering peaks observed in the IF-WS_2 and nanotube RR spectra are given in Table III. Unfortunately, the $2 \times LA$ (352 cm^{-1}) band overlaps the first-order E^1_{2g} peak (356 cm^{-1}). Therefore, the LA mode (178 cm^{-1}) will overlap the second-order $E^1_{2g} - LA$ (352 − 178 = 174 cm^{-1}) band. Consequently, the scattering of the first-order, non-zone-center LA mode could not be resolved in the RR spectra of WS_2 nanoparticles. Nevertheless, we believe that the higher relative intensity of the band at 172 cm^{-1} in the spectra of the IF-WS_2 and nanotubes, compared to that of the 2H bulk sample, is due to the disorder-induced peak arising from non-zone-center LA phonons (see Fig. 6).

Inclusion of disorder could also be the cause for the appearance of the other new peaks at 250 and 498 cm^{-1} in the Raman spectra for the MoS_2 nanoparticles (the 250 cm^{-1} peak corresponds to scattering of a zone-edge phonon, while the peak at 498 cm^{-1} would correspond to a second-order scattering process involving two such

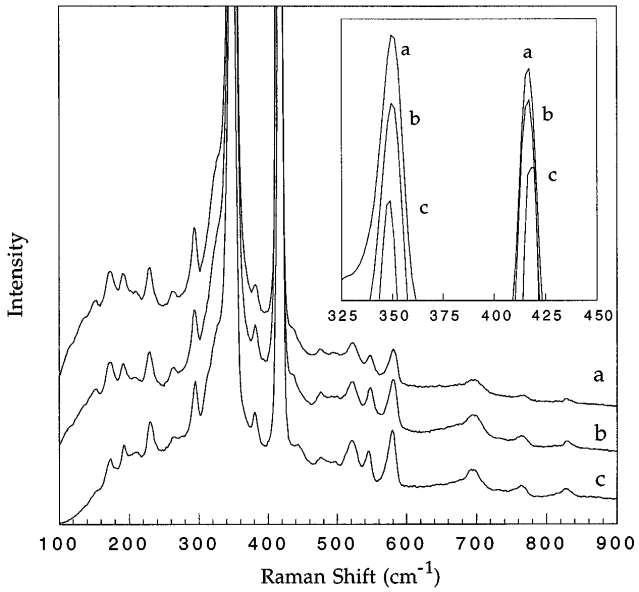

FIG. 6. Resonance Raman (RR) spectra excited by the 6328 Å (1.96 eV) laser line showing SOR bands of several WS_2 nanoparticle samples: WS_2 nanotubes 150–200 Å in diameter and 1500–3000 Å in length (a); IF-WS_2 1500–2000 Å (b); bulk WS_2 (c).

zone edge phonons), and at 152 cm^{-1} for the spectra for WS_2 nanoparticles. An additional mechanism which could bring about first-order zone-edge scattering is the zone-folding due to the formation of a superlattice. A zone-folding process can activate formerly inactive zone-edge phonons while preserving the k-selection rule. The folding of the BZ along Γ-M (or Γ-K) would cause the M point to coincide with the Γ point, so that the $LA(M)$ phonons would become Raman active in a first-order process. As a result of the increased surface area for smaller particles, as well as lattice-strain relief in the IF, such a lattice distortion/reconstruction into a superlattice may occur in the MS_2 samples of the present study.

IV. CONCLUSION

In conclusion, optical absorption measurements show that the semiconductivity of MoS_2 and WS_2 is preserved in the IF and nanotube structures. Nevertheless, the positions of the A and B excitons are altered in comparison to those in the 2H bulk samples. A systematic study of the effect of the IF size and the number of atomic layers reveals that the position of the excitons is dependent on the number of IF layers (n) rather than on the particle size. The off-resonance and resonance Raman spectra of the fullerene-like and nanotube materials show a close correspondence to the corresponding spectra for the 2H single-crystal system. However, the first-order peaks are broadened and, under resonance conditions, new peaks are observed. The new peaks are assigned to disorder-induced zone-edge-phonons.

ACKNOWLEDGMENTS

The authors wish to thank Y. Feldman and M. Homyonfer for sample preparation and Dr. Don Heiman for helpful discussions and generous use of optical equipment at the Francis Bitter Magnet Laboratory. This work was supported by a NEDO (Japan) International collaboration program. The MIT authors acknowledge support from NSF 95-10093 DMR.

REFERENCES

1. R. Tenne, L. Margulis, M. Genut, and G. Hodes, Nature (London) **360**, 444 (1992).
2. L. Margulis, G. Salitra, R. Tenne, and M. Talianker, Nature (London) **365**, 113 (1993).
3. Y. Feldman, E. Wasserman, D. J. Srolovitz, and R. Tenne, Science **267**, 222 (1995).
4. Y. Feldman, G. L. Frey, M. Homyonfer, V. Lyakhovitskaya, L. Margulis, H. Cohen, G. Hodes, J. L. Hutchison, and R. Tenne, J. Am. Chem. Soc. **118**, 5362 (1996).
5. M. Homyonfer, B. Alperson, Y. Rosenberg, L. Sapir, H. Cohen, G. Hodes, and R. Tenne, J. Am. Chem. Soc. **119**, 2693 (1997).
6. M. Hershfinkel, L. A. Gheber, V. Voltera, J. L. Hutchison, L. Margulis, and R. Tenne, J. Am. Chem. Soc. **116**, 1914 (1994).
7. G. L. Frey, S. Ilani, M. Homyonfer, Y. Feldman, and R. Tenne, Phys. Rev. B **57**, 6666 (1998).
8. G. L. Frey, R. Tenne, M. J. Matthews, M. S. Dresselhaus, and G. Dresselhaus, unpublished.
9. R. Coehoorn, C. Hass, J. Dijkstra, and C. J. F. Flipse, Phys. Rev. B **35**, 6195 (1987).
10. R. Coehoorn, C. Hass, and R. A. de Groot, Phys. Rev. B **35**, 6203 (1987).
11. C. Ballif, P. E. Regula, M. Remskar, R. Sanjinés, and F. Lévy, Appl. Phys. A **62**, 543 (1996).
12. A. R. Beal, J. Phys. C **12**, 881 (1979).
13. J. V. Acrivos, W. Y. Liang, J. A. Wilson, and A. D. Yoffe, J. Phys. C **4**, L18 (1971).
14. A. D. Yoffe, Adv. Phys. **42**, 173 (1993).
15. F. Consadori and R. F. Frindt, Phys. Rev. B **3**, 4893 (1970).
16. B. L. Evans and P. A. Young, Proc. R. Soc. A **298**, 7 (1967).
17. J. P. Wilcoxon and G. A. Samara, Phys. Rev. B **51**, 7299 (1995).
18. M. W. Peterson and A. J. Nozik, in *Photoelectrochemistry and Photovoltaics of Layered Semiconductors*, Vol. 14 of *Physics and Chemistry of Materials with Layered Structures*, edited by A. Aruchamy (Kluwer Academic Publishers, Dordrecht, The Netherlands, 1992), p. 297.
19. K. Kobayashi and J. Yamauchi, Phys. Rev. B **51**, 17 085 (1995).
20. T. J. Wieting and J. L. Verble, Phys. Rev. B **3**, 4286 (1971).
21. J. M. Chen and C. S. Wang, Solid State Commun. **14**, 857 (1974).
22. T. Sekine, K. Uchinokura, T. Nakashizu, E. Matsuura, and R. Yoshizaki, J. Phys. Soc. Jpn. **53**, 811 (1984).
23. J. L. Verble and T. J. Wieting, Phys. Rev. Lett. **25**, 362 (1970).
24. A. M. Stacy and D. T. Hodul, J. Phys. Chem. Solids **46**, 405 (1985).
25. C. Sourisseau, F. Cruege, and M. Fouassier, Chem. Phys. **150**, 281 (1991).
26. N. Wakabayashi, H. G. Smith, and R. M. Nicklow, Phys. Rev. B **12**, 659 (1975).